Bio-Design and Manufacturing (2025) 8:275–287
https://doi.org/10.1631/bdm.2400259

RESEARCH ARTICLE

# A design strategy for long-term stability of porous PEEK implants by regulation of porous structure and in vivo mechanical stimulation

Yingjie Liu[1,2] · Ling Wang[1,2] · Jie Zhang[3,4] · Shuguang Liu[3] · Jibao Zheng[1,2] · Jianfeng Kang[5] · Enchun Dong[1,2] · Changning Sun[1,2] · Ruhan A[6] · Chaozong Liu[7] · Chuncheng Yang[8] · Dichen Li[1,2]

Received: 1 July 2024 / Accepted: 21 September 2024 / Published online: 1 March 2025


**Abstract**

The bioinert nature of polyether ether ketone (PEEK) material limits the widespread clinical application of PEEK implants. Although the porous structure is considered to improve osseointegration of PEEK implants, it is hardly used due to its mechanical properties. This study investigated the combined influence of the porous structure and in vivo mechanical stimulation on implantation safety and bone growth based on finite element analysis of the biomechanical behavior of the implantation system. The combined control of pore size and screw preloads allows the porous PEEK implant to achieve good osseointegration while maintaining a relatively high safety level. A pore size of 600 μm and a preload of 0.05 N·m are the optimal combination for the long-term stability of the implant, with which the safety factor of the implant is >2, and the predicted percentage of effective bone growth area of the bone-implant interface reaches 97%. For further clinical application, PEEK implants were fabricated with fused filament fabrication (FFF) three-dimensional (3D) printing, and clinical outcomes demonstrated better bone repair efficacy and long-term stability of porous PEEK implants compared to solid PEEK implants. Moreover, good osteointegration performance of 3D-printed porous PEEK implants was observed, with an average bone volume fraction >40% three months after implantation. In conclusion, 3D-printed porous PEEK implants have great potential for clinical application, with validated implantation safety and good osseointegration.

✉ Ling Wang
menlwang@xjtu.edu.cn

✉ Dichen Li
dcli@xjtu.edu.cn

1 State Key Laboratory for Manufacturing Systems Engineering, School of Mechanical Engineering, Xi'an Jiaotong University, Xi'an 710049, China

2 National Medical Products Administration (NMPA) Key Laboratory for Research and Evaluation of Additive Manufacturing Medical Devices, Xi'an Jiaotong University, Xi'an 710049, China

3 Stomatological Hospital of Southern Medical University, Guangzhou 510280, China

4 Department of Oral and Maxillofacial Surgery, Center of Stomatology, Xiangya Hospital, Central South University, Changsha 410000, China

5 School of Mechatronic Engineering and Automation, Foshan University, Foshan 528225, China

6 Center for Medical Device Evaluation of NMPA, Beijing 100076, China

7 Institute of Orthopaedic & Musculoskeletal Science, University College London, Royal National Orthopaedic Hospital, Stanmore HA7 4LP, UK

8 Shaanxi Jugao-AM Technology Co., Ltd., Xi'an 714026, China

**Graphical abstract**

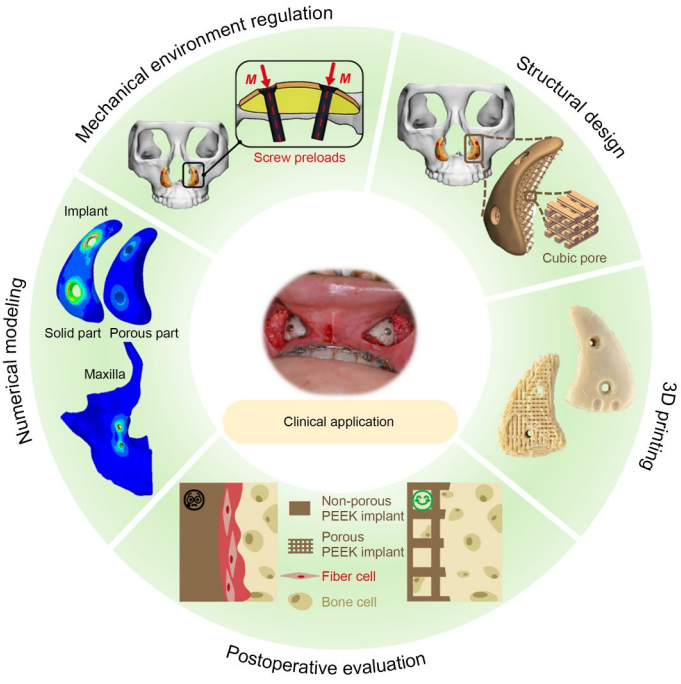


**Keywords** Porous polyether ether ketone (PEEK) implant · Osteointegration · Interface biomechanics · Maxillofacial implants · Finite element analyses · Fused filament fabrication (FFF) 3D printing

## 1 Introduction

Polyether ether ketone (PEEK), an ideal material for bone tissue repair, has been widely utilized in orthopedic and dental fields, having the potential to replace titanium alloys [1]. In recent years, three-dimensional (3D) printed PEEK implants have been increasingly used for clinical applications due to their ability to match the geometric features and mechanical properties of patients' anatomy [2]. Among these applications, the use of 3D-printed PEEK implants for the reconstruction of maxillofacial bone has received particular attention [3], because bone autografts, the gold standard, usually cannot appropriately recapitulate the maxillofacial contours for an aesthetic appearance and have an unpredictable resorption rate [4].

Despite their potential benefits, further application of 3D-printed PEEK implants is hindered by the bioinert nature of PEEK itself, associated with poor osseointegration post-implantation [5]. Various strategies, including composite formation, surface modification, drug loading, and porous structure construction, have been explored to improve the osseointegration of PEEK implants [6]. However, except for the construction of porous structures, all others alter the properties of PEEK itself, creating additional difficulties for a wide range of clinical applications, as the long-term effects of these changes on the human body need to be demonstrated first [7].

The porous structure of PEEK implants can be fabricated by traditional methods such as porogen templating, gas foaming, and sulfonation, and 3D printing techniques like fused filament fabrication (FFF) and selective laser sintering (SLS). Porogen templating [8] and gas foaming [9] can produce porous PEEK structures with pore sizes ranging from tens to hundreds of microns, while sulfonation [10] can produce nanometer-sized pore structures, all shown to be beneficial for osseointegration. However, traditional methods lack precise control of pore sizes, architecture, and distribution to meet individual requirements for bone defect repair in various areas. Thus, 3D printing techniques are gradually replacing the traditional methods. Zheng et al. [11] prepared PEEK composite scaffolds by FFF printing with a tunable elastic modulus of 50.6–624.7 MPa by changing pore sizes from 200 to 2000 μm. Wang et al. [12] fabricated PEEK scaffolds by SLS printing with an elastic modulus range of 42.17–512.12 MPa by controlling volume fractions of 20% – 40%. Both were similar to the variation range of natural cancellous bone [13]. Similarly, Gummadi [14], Du [15], Spece [16], and Jia [17] et al. have achieved highly controllable mechanical properties

of PEEK scaffolds by controlling pore sizes, porosity, pore architecture, and pore distribution, respectively. In addition, cell adhesion and bone formation of 3D-printed porous PEEK scaffolds were validated by in vitro cell cultures and in vivo animal implantation studies [11, 17, 18].

In summary, existing research on the design of porous PEEK structures focuses on an isolated aspect rather than combined mechanisms. Specifically, the influence of porous structures on mechanical properties and bone growth was investigated separately, although changes in the mechanical properties of the implant can affect the stress distribution in the surrounding bone tissue and cause changes in bone growth [19]. Meanwhile, most in vivo animal studies of porous PEEK scaffolds were conducted in regions bearing low stress, and the effect of in vivo mechanical loading on osseointegration was often ignored. However, mechanical loads are a crucial consideration in the prosthetic design process for clinical applications. On the one hand, the porous structure may compromise the safety of the implant, and on the other hand, variations in mechanical stimuli can influence bone growth. Further, there is limited research on porous PEEK implants for clinical application. The combined influence of the porous structure and in vivo mechanical loads on the implantation safety and osseointegration performance of porous PEEK implants has not been adequately studied so far. In addition, to date, there are no reported clinical applications of 3D-printed porous PEEK implants.

This study used paranasal implants as the research object, aiming to investigate the combined influence of the pore structure and in vivo mechanical stimuli on implantation safety and osseointegration based on finite element (FE) analysis of the biomechanical behavior of the implantation system. The clinical applications of 3D-printed PEEK implants for paranasal augmentation were carried out and evaluated to further validate the clinical efficacy of the porous PEEK structure.

## 2 Materials and methods

### 2.1 Materials and equipment

The raw material used for manufacturing the prosthesis and scaffold in this study was biological grade PEEK powder (150PF, Victrex plc, Lancashire, UK). This powder was fed into a twin-screw extruder and extruded into filaments with a diameter of 1.75 mm, then printed using an FFF 3D printer (Surgeon Plus, Jukang Gobo Medical Technology, Shaanxi, China). The printing parameters used in this study were as follows: nozzle diameter of 0.4 mm, nozzle temperature of 420 °C, printing speed of 20 mm/s, and a layer height of 0.2 mm.

### 2.2 Compression test for the porous PEEK sample

To investigate changes in the mechanical properties of porous PEEK structures with different pore sizes, this study prepared cubic pore PEEK scaffold specimens with pore sizes of 0, 200, 400, 600, 800, and 1000 μm ($n$=6, length, width, and thickness=10 mm each) for compression testing to obtain the equivalent mechanical properties of porous PEEK structures with different pore sizes. Uniaxial compression tests were conducted using a universal mechanical testing machine (CMT4304, MTS Corp, USA) at a compression speed of 3 mm/min [11]; the compression direction followed the vertical printing direction of the scaffolds. The force–displacement curves during the compression of porous structures were recorded and converted into stress–strain curves based on the dimensional characteristics of the porous structures. The elastic modulus was calculated based on the slope of the initial linear stage of the stress–strain curve. The yield strength was calculated when there was a measurable change in the slope.

### 2.3 Biomechanical analysis of porous PEEK implants and interfacial bone

#### 2.3.1 Design of porous PEEK implants for paranasal augmentation

Paranasal defects are a common type of midfacial deformity caused by maxillofacial trauma or developmental abnormalities of the maxilla [20, 21]. The clinical data for this study were sourced from the Third Affiliated Hospital of Southern Medical University (Guangzhou, China). Patients underwent computed tomography (CT) scans of the head; CT images were used to construct models of maxillofacial bones in MIMICS software (Version 20.0, Materialize, Inc., Leuven, Belgium) for assessing paranasal defects and the geometric design of the implants, as shown in Figs. 1a and 1b). Using anatomical consistency as a design criterion [22], the implant models were established on both sides of the paranasal area, and a smooth transition between the implant and the maxillary bone was achieved. The outer region in contact with the soft tissue was designed as a solid structure with a thickness of about 1 mm to prevent soft tissue from invading the porous structure. This part of the PEEK implant will be referred to as the "solid part" henceforth. The bottom region of the implant in contact with the host bone was designed as uniform cubic porous structures. This part of the PEEK implant will be referred to as the "porous part" henceforth. For a pore size of the porous part equaling zero, the entire PEEK implant is solid. To prevent implant rotation, bilateral anchoring screws, with a diameter of 2 mm, a length of 10 mm, and a pitch of 0.4 mm, supplied by Waston Medical (Changzhou, China), were used for fixation.

### 2.3.2 FE model of the PEEK implant, the maxillofacial bone, and screws

We established a numerical model of the bone in the paranasal area and the prosthesis using the FE method in ABAQUS software (Version 6.14, ABAQUS Inc., USA). As shown in Fig. 1c, the FE model in this study included three parts: the unilateral maxillary bone, the implant, and two screws. Table 1 lists the mechanical properties of each part, assuming that all materials are homogeneous, isotropic, and linearly elastic. The PEEK implant consists of a solid part and a porous part, as described in Sect. 2.3.1. To save computational costs, the equivalent material properties of porous PEEK structures obtained from the compression tests described in Sect. 2.2 were used for the porous part of the PEEK, with feasibility confirmed in previous studies [24, 25]. The model was meshed with quadratic 10-node tetrahedral elements (C3D10), and a sensitivity analysis was conducted until <5% change in the maximum von Mises stress was obtained by mesh refinement. Finally, we set a mesh size of 0.25 mm.

The boundary conditions and loads on the model were set according to the mechanical environment of the prosthesis in the human body. The paranasal region of the maxillary bone bears relatively low stresses (<1 MPa) under normal

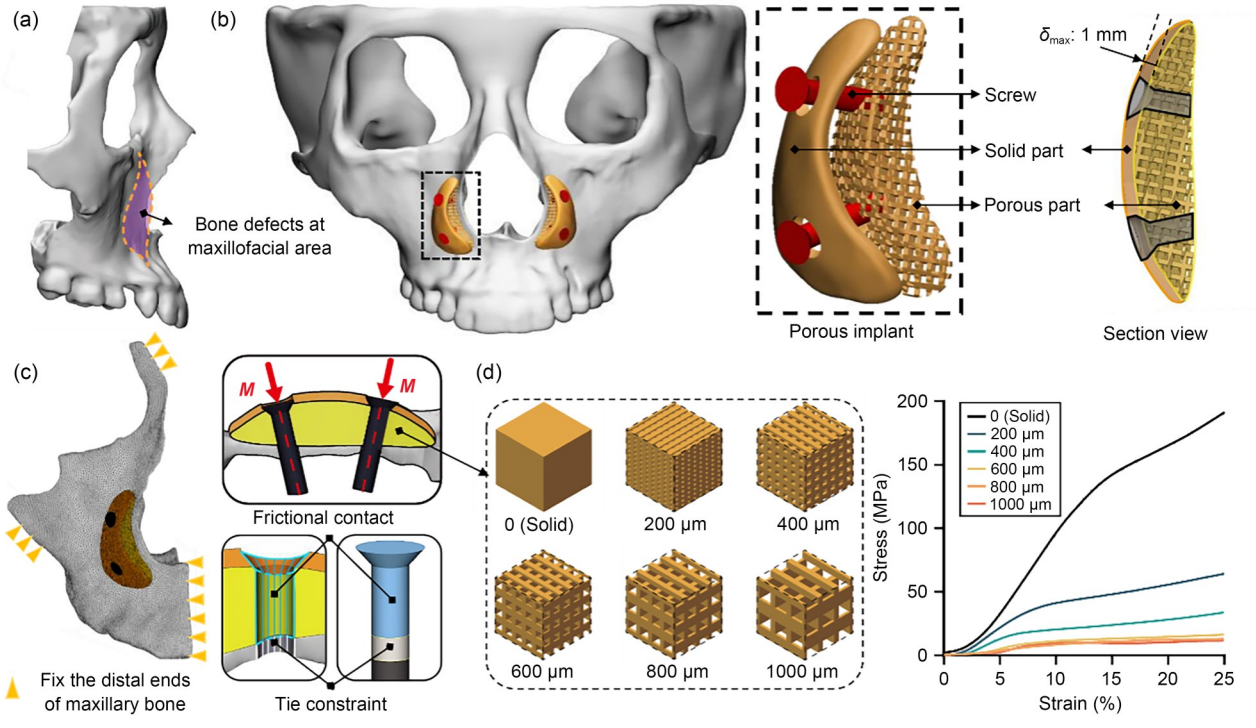


**Fig. 1** 3D model of the maxillofacial bone and porous PEEK implants and FE model for this study. (a) Reconstructed maxillofacial bone with paranasal defects. (b) Porous PEEK implants for paranasal augmentation. Each PEEK implant consisted of a solid part and a porous part, and was fixed on the maxillofacial bone by two screws. (c) Boundary conditions, contacts, and interactions of the FE model. (d) Schematic diagram of the 3D unit cells of porous PEEK structures with different pore sizes and their corresponding representative stress–strain curves, which could be divided into three stages: elastic, plateau, and densification. PEEK: polyether ether ketone; FE: finite element

**Table 1** Mechanical properties of the materials used in the FE model

| Component | Pore size (μm) | Elastic modulus (MPa) | Poisson's ratio | Yield strength (MPa) | Reference |
|---|---|---|---|---|---|
| PEEK | 0 | 1305 | 0.3 | 148 | / |
| | 200 | 551 | 0.3 | 41 | |
| | 400 | 414 | 0.3 | 23 | |
| | 600 | 190 | 0.3 | 12 | |
| | 800 | 150 | 0.3 | 11 | |
| | 1000 | 127 | 0.3 | 10 | |
| Maxillary bone | / | 12 000 | 0.3 | 88 | [23] |
| Titanium screws | / | 110 000 | 0.3 | 850 | [23] |

FE: finite element; PEEK: polyether ether ketone

physiological conditions [26, 27], and the tightening loads on the screws were considered major loads. The area where the maxillary bone connects with adjacent bones was fully constrained. Bonding constraints were applied to the interface between the screws and the maxillary bone to ensure the lack of relative displacement between the screws and the host bone. The "Bolt Load" feature in ABAQUS was used to apply tightening forces to the two screws, with the tightening torque transformed into input force using the following formula:

$$F = 1000M/(K{\cdot}d). \quad (1)$$

In the formula, $F$ represents the tightening force in Newtons (N); $M$ is the tightening torque in Newton-meters (N·m); $K$ is the torsional coefficient (0.3); $d$ is the nominal diameter of the thread, set as 2 mm. The tightening loads of the two screws were consistent for all models.

#### 2.3.3 Parameterized study of implantation safety and bone growth

The in vivo mechanical performance and stress distribution of each implant component with various pore sizes (0–1000 μm) and screw preloads (0.01–0.09 N·m) were investigated. The safety factors of each component were assessed by comparing the ratio of the maximum stress obtained through FE analysis to the yield stress. The strain distributions of the bone-implant interface and the bone-screw interface were extracted to assess bone growth based on Wolff's law. To predict the osseointegration performance of the implant, we calculated the effective bone growth area at the interface. After evaluating the combined influence of the pore structure and in vivo mechanical loads, the optimal pore size and screw preload were selected to achieve both good implantation safety and osseointegration performance for further clinical applications.

### 2.4 Clinical applications for PEEK implants

Fifteen patients (14 females and 1 male) with an average age of (26±3) years were recruited at the Third Affiliated Hospital of Southern Medical University. The 3D-printed PEEK implants were approved by the State Key Laboratory for Manufacturing Systems Engineering. Patient selection and inclusion criteria were described in detail in our previous study [28]. Patients were randomly assigned to two different groups: one group (7 patients) underwent treatment with 3D-printed solid PEEK implants and the other group (8 patients) with 3D-printed porous PEEK implants with the optimal pore size obtained in Sect. 2.3.

All patients underwent surgery at the Third Affiliated Hospital of Southern Medical University. Patients were followed up at 3 days, 3 months, and 6 months postoperatively; a CT scan of the head was performed each time. The average Hounsfield unit (HU) values of the bone-implant interface and the PEEK prostheses were calculated based on the CT scans. The maxillofacial bone, PEEK prostheses, and the newly formed bone tissue were 3D reconstructed. Next, we obtained the bone volume fraction (BV/TV), which represented the ratio of newly formed bone volume to the pore volume of the prosthesis and could directly reflect changes in the newly formed bone volume.

### 2.5 Statistical analysis

Experimental data are presented as mean±standard deviation. Statistical analyses were performed using GraphPad Prism 9.0 software (GraphPad Software, USA) or Origin 2024 software (Origin Software, USA). Data were analyzed using one-way analysis of variance (one-way ANOVA) and Tukey's multiple comparison test. The thresholds for statistical significance were $^{*}P<0.05$ and $^{**}P<0.01$.

## 3 Results

### 3.1 Stress distribution on the implants

The biomechanical behavior of the PEEK implant, maxillary bone, and screws was analyzed based on the FE method. The influence of various pore structures and preloads was mainly concentrated on the stress values of each component, and there was little difference in the stress distribution. The representative stress distributions of each component with a pore size of 600 μm and a preload of 0.05 N·m are shown in Fig. 2. The results indicated that the von Mises stress in the maxillary bone was mainly distributed at the bone-implant interface, with the maximum stress found at the edge of the screw hole. The farther from the screw holes, the lower the von Mises stress value. In addition, the average stress in the region between the two screws was one-fifth of the maximum stress. For the PEEK implant, stress was also concentrated around the screw holes, and the maximum stress in the solid part was nearly six times higher than in the porous part.

### 3.2 Safety analyses

Figure 2 shows the variation of the maximum von Mises stress of each component under the combined influence of pore sizes and preloads. The maximum stress of each component increased with higher preload for different pore sizes; the increase was proportional to the stress value of the component itself. The maximum stress of the maxillary bone and the screws increased with pore size. The increase in the maximum stress of the solid part of the PEEK implant was not

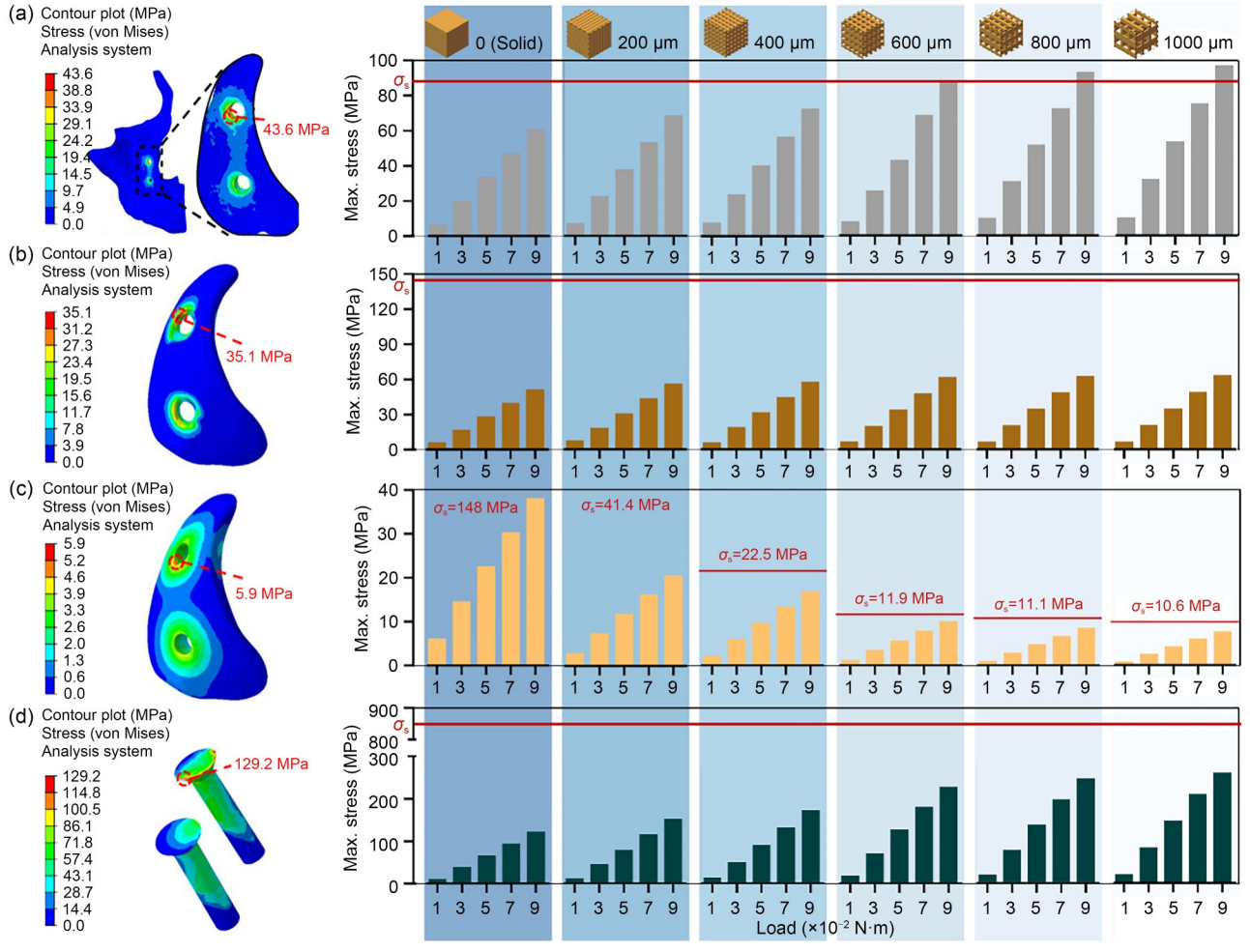


**Fig. 2** Representative von Mises stress distribution and the predicted maximum von Mises stress at various pore sizes and preloads of the maxillary bone with a zoomed-in area of interfacial bone (a), the solid part of the PEEK implant (b), the porous part of the PEEK implant (c), and the screws (d). The representative von Mises stress distribution is under a pore size of 600 μm and preload of 0.05 N·m. The yield strength of each component is marked with a red line. For the porous part of the PEEK implant, the yield strength changed with pore size. PEEK: polyether ether ketone

obvious, while an obvious decrease was shown in the maximum stress of the porous part of the PEEK implant with the increasing pore size. The maximum stress on the maxillary bone exceeded its yield strength for a preload >0.09 N·m and a pore size >600 μm, which indicated the possibility of bone fracture after implantation.

The variation in the safety factor of each component under the combined influence of pore sizes and preloads is shown in Fig. 3. The safety factor of the screws was higher than that of the other components. Further, the influence of preload on the safety factor was more obvious. Increasing the preload decreased the influence of the pore size on the safety factor. For a preload >0.07 N·m, the safety factor of the porous part of the PEEK implant and the maxillary bone was below 2 at all pore sizes. For the porous part of the implant, the increase in pore size resulted in a simultaneous decrease in the maximum stress and yield strength, which ultimately decreased the safety factor. Moreover, the influence of the pore size on the porous part of the implant was highest among all components. Taken together, smaller pore size and lower preload were more beneficial to the implantation safety of all components.

### 3.3 Strain distribution of the interfacial bone and bone growth analysis

Figure 4 shows the strain distribution of the bone-implant interface and the bone-screw interface under different pore sizes and preloads. Under the same conditions, the average strain at the bone-screw interface was higher than that at the bone-implant interface, and the maximum strain at the bone-implant interface was primarily concentrated around the two screw holes. Further, the bone growth of the interfacial bone was predicted by Wolff's law, defining the effective bone growth area as that for a strain between 50 and 3000 με. The bone growth of the bone-implant interface was related

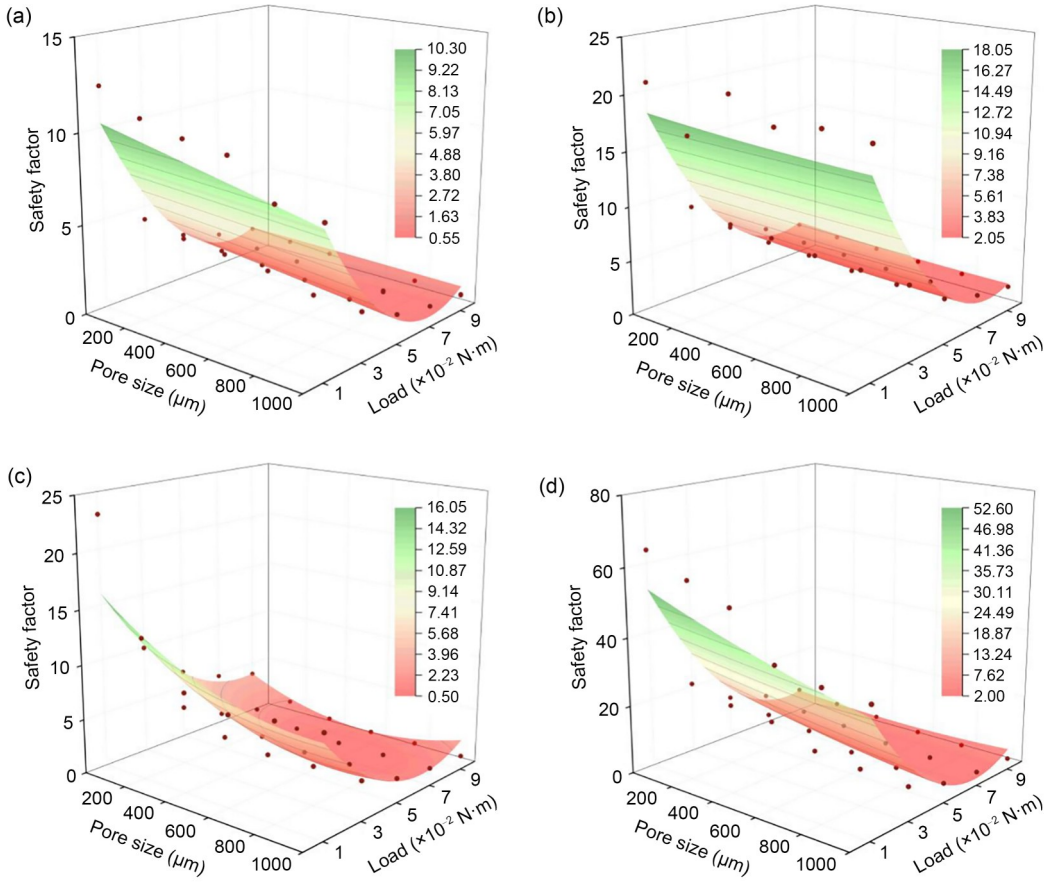


**Fig. 3** Combined influence of pore size and preload on the safety factor of the maxillary bone (a), the solid part of the PEEK implant (b), the porous part of the PEEK implant (c), and the screws (d). PEEK: polyether ether ketone

to the osseointegration of the PEEK implant, while the bone growth of the bone-screw interface was related to the long-term stability of the screw connections [29].

For the bone-implant interface, the increase in pore size markedly increased the effective bone growth area for a low preload. For a preload of 0.01 N·m, the effective bone growth area with a pore size of 600 μm was three times larger than that with a pore size of 0 μm (solid implant). An increase in the preload also increased the effective bone growth area. For a solid implant, the preload had to be increased to >0.07 N·m to maintain most of the bone-implant interface within the effective bone growth range. However, when the preload and the pore size exceeded a certain level, the strain at the bone-implant interface near the screw holes got >3000 με, which decreased the effective bone growth area. For the bone-screw interface, the entire interface was within the effective bone growth range under the minimum pore size (0 μm) and preload (0.01 N·m). With increasing pore size and preload, the effective bone growth area decreased for a strain in the peripheral area of the interface >3000 με.

Next, we calculated the percentage of the effective bone growth area in the bone-implant interface and the bone-screw interface, as shown in Fig. 5. The percentage in the bone-implant interface reached a maximum of 97.4% for a pore size of 600 μm and a preload of 0.05 N·m, or when the pore size was 200 μm and the preload was 0.07 N·m. However, the percentage of effective bone growth area in the bone-screw interface with a pore size of 600 μm and a preload of 0.05 N·m (90.2%) was higher than that with a pore size of 200 μm and a preload of 0.07 N·m (83.0%), which was beneficial to the screw fixation and the long-term stability of the implant. Considering the combined influence of the pore size and preload on implantation safety and osseointegration, a pore size of 600 μm and a preload of 0.05 N·m were chosen as the optimal combination to improve bone growth while maintaining safety. With this optimal combination, the safety factor of each component was >2, and the percentage of effective bone growth area in the bone-implant interface was 97.4%.

## 3.4 Clinical outcomes

A total of 15 clinical applications have been carried out, including the solid PEEK implant group (7 patients) and the porous PEEK implant group (8 patients). The average thickness of PEEK implants fabricated using FFF 3D printing

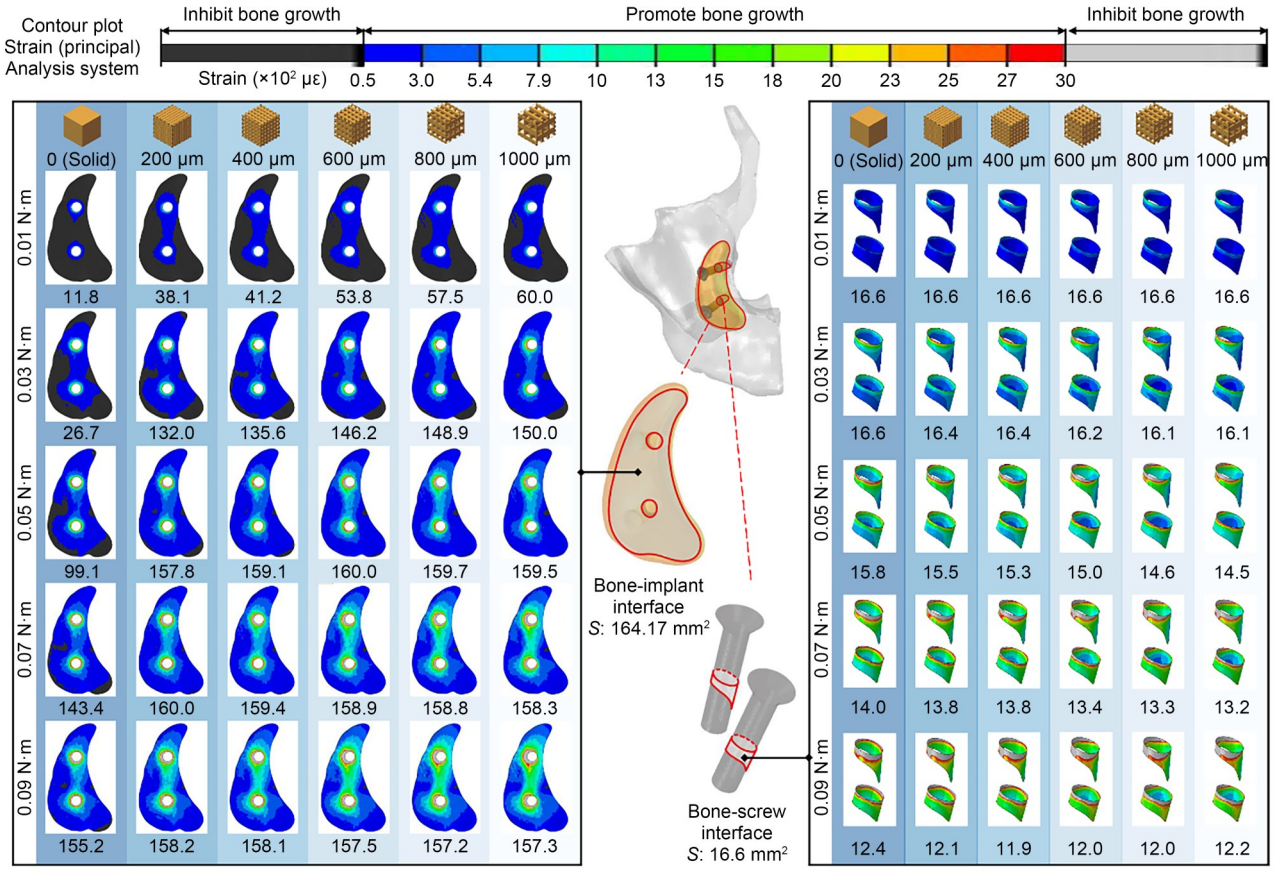


**Fig. 4** Predicted strain distribution and effective bone growth area of the bone-implant interface and the bone-screw interface with various pore sizes and preloads. The data under each strain distribution diagram show the effective bone growth area in $mm^2$

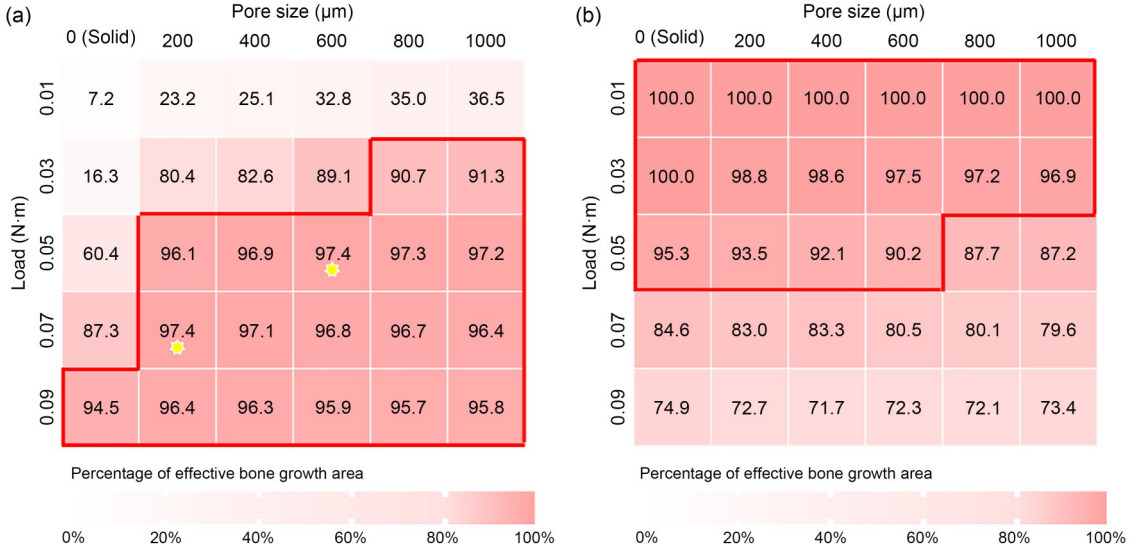


**Fig. 5** Percentage of the effective bone growth area under various pore sizes and preloads of the bone-implant interface (a) and the bone-screw interface (b). Combinations of pore size and preload resulting in a percentage >90% are enclosed by a red line. The combinations of pore size and preload that resulted in the highest percentage of the effective bone growth area of the bone-implant interface are marked by a yellow asterisk

technology was (5±1.5) mm. A uniform cubic pore structure design with a pore size of 600 μm was used for porous PEEK implants, as shown in Fig. 6a. Different preloads were applied on the screws to the two groups, 0.07 N·m preload to the solid PEEK implant group and 0.05 N·m preload to the porous PEEK implant group, according to the results

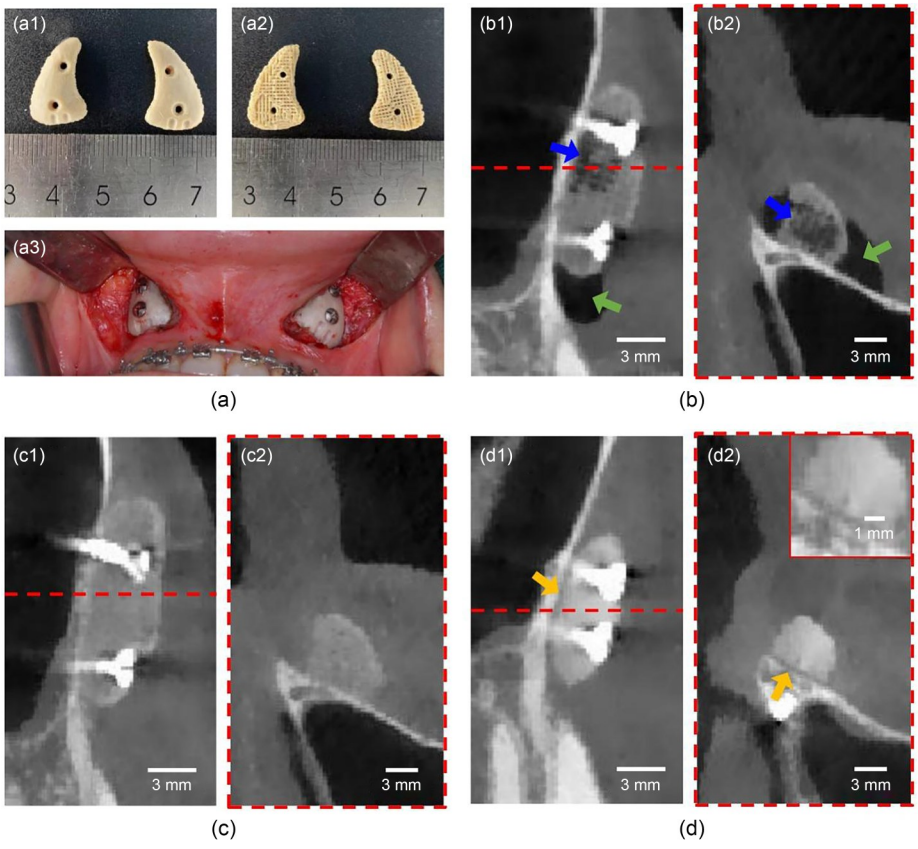


**Fig. 6** Representative intraoperative photos and postoperative CT images. (a) Front (a1) and back (a2) of 3D-printed porous PEEK implants. (a3) PEEK prostheses after implantation. (b) CT images of the 3D-printed porous PEEK implant at 3 days post-intervention: (b1) coronal plane; (b2) sagittal plane. The blue arrow indicates the porous structure and the green arrow points to the incisions. (c) CT images of the 3D-printed porous PEEK implant at 3 months post-intervention: (c1) coronal plane; (c2) sagittal plane. (d) CT images of the 3D-printed solid PEEK implant at 3 months post-intervention: (d1) coronal plane; (d2) sagittal plane. The yellow arrow points to the gap between the bone and the implant. PEEK: polyether ether ketone; CT: computed tomography

in Sect. 3.3. During the surgical procedure, all implants in both groups perfectly matched the geometric shape of the defect maxillary bone, and no implant migration, extrusion, or rupture occurred post-surgery.

Figures 6b–6d show representative postoperative CT images of the porous and solid PEEK implant groups. The characteristics of the porous structure of the porous PEEK implant could be clearly observed on the CT at 3 days after surgery (Fig. 6b), while no radiolucent area of the porous structure was observed in the same region on the CT at 3 months after surgery (Fig. 6c), indicating new bone formation within the porous structure of the porous PEEK implant. However, the bone growth and osteointegration performance of the solid PEEK implant was not good, as there was a gap between the solid implant and the maxillary bone on the CT at 3 months after surgery (Fig. 6d).

Based on CT images, we reconstructed 3D models of PEEK implants and the new bone within the implants of the porous PEEK implant group 3 months after surgery, as shown in Fig. 7a. New bone formation was mainly concentrated in the central area of the implants, especially around the screw holes, which was consistent with the effective bone growth region results obtained in Sect. 3.3 (Fig. 4). The average BV/TV of the porous part of porous PEEK implants was calculated, reaching 42.2% after 3 months and 59.9% after 6 months. We also observed a significant increment in the HU value of the porous part of porous PEEK implants, indicating an increasing new bone formation within porous PEEK implants (Fig. 7c).

To further compare bone growth at the bone-implant interface between implant groups, we calculated the change in HU value at the interface (Figs. 7d and 7e). The HU value at the interface of patients in the porous PEEK implant group decreased at 3 months postoperatively but returned to preoperative values at 6 months postoperatively (Fig. 7d), suggesting good bone growth. However, the HU value at the interface of patients in the solid PEEK implant group significantly decreased at both 3 and 6 months postoperatively (Fig. 7e). In conclusion, based on CT images and the change in HU value, the osseointegration performance of 3D-printed porous PEEK implants was better than that of 3D-printed solid PEEK ones.

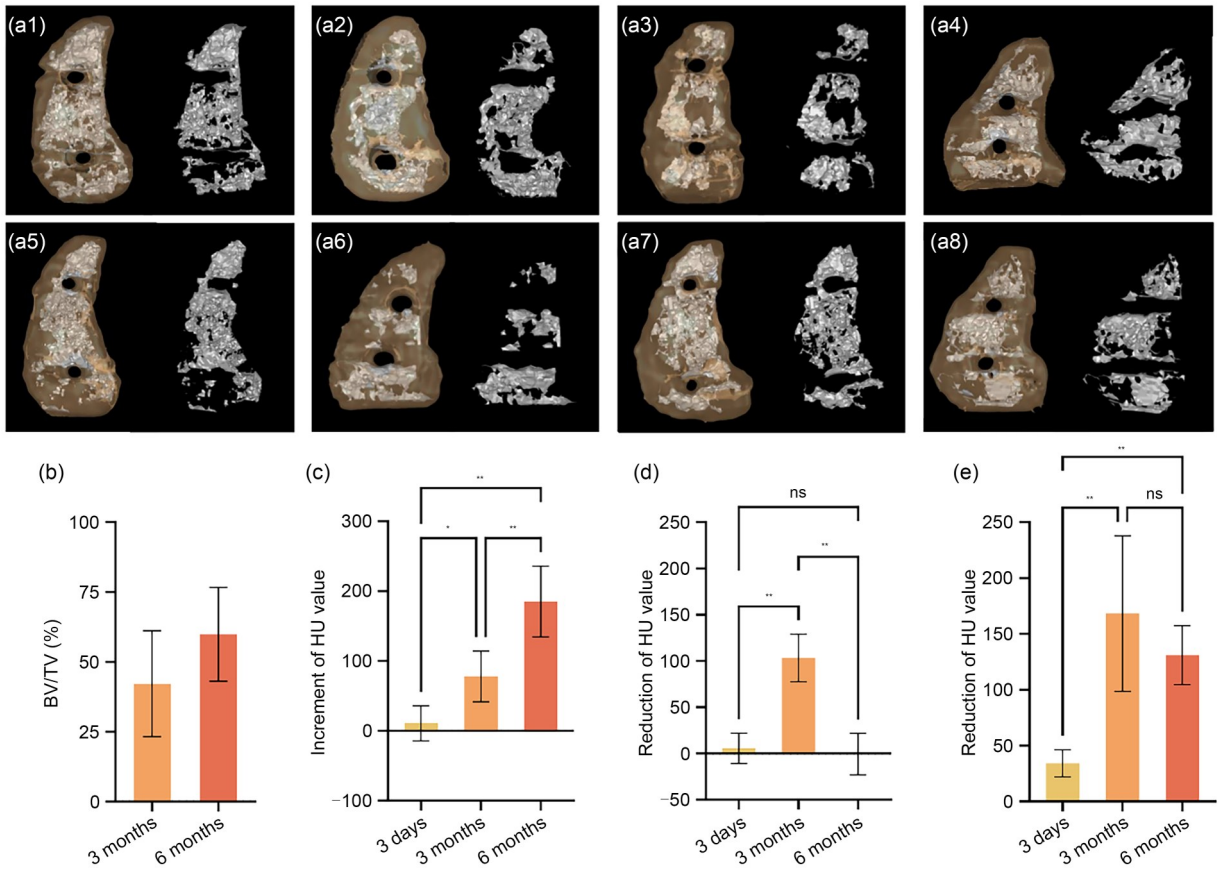


**Fig. 7** Analysis of bone growth after implantation. (a) Reconstructed 3D models of PEEK implants with new bone (left) and new bone extracted separately (right) based on the CT images 3 months after surgery. (a1–a8) refer to eight different patients in the porous PEEK implant group. (b) BV/TV of porous implants 3 and 6 months after implantation. (c) Increment in HU value of the porous part of porous PEEK implants at different time points after surgery. (d) Decrease in HU value of the bone-implant interface of patients in the porous PEEK implant group at different time points after surgery. (e) Decrease in HU value of the bone-implant interface of patients in the solid PEEK implant group at different time points after surgery. The baseline HU value of the comparison in (c–e) corresponds to that of the relevant object shortly before implantation. Data are presented as mean±standard deviation ($n$=8 for (b–d); $n$=7 for (e)); $^{*}P<0.05$, $^{**}P<0.01$, ns: not significant. PEEK: polyether ether ketone; CT: computed tomography; HU: Hounsfield unit; BV/TV: bone volume fraction, representing the ratio of newly formed bone volume to the pore volume of the prosthesis

## 4 Discussion

Despite the broad use of PEEK implants, most are solid structures. There are only a few reports [30, 31] on the clinical application of porous PEEK implants and none were manufactured using 3D printing. A classic example of one of the few clinically used porous PEEK implants is the PEEK interbody fusion cage (COHERE®) [31]; the pores created by porogen templating enhance bone bonding and spinal fusion. However, the porous structure of the PEEK Interbody Fusion Cage does not allow a free design in terms of pore architecture, size, or distribution, all playing an important role in osseointegration. Several studies focused on the design of the porous structure of PEEK prostheses, but a few research works have shown the importance of this design. Moiduddin et al. [32] analyzed the stress distribution and the deformation of a cranial PEEK implant with a uniform diamond pore structure (pore size: 1350 μm; porosity: 70%) under a physiological load by FE. Sharma et al. [30] compared the mechanical behavior of PEEK orbital mesh implants with three different porous constructs. Although these studies considered the relationship between porous structure design and implantation safety, the influence of the porous structure on bone growth and osseointegration performance was not investigated. In this study, the structural design of porous PEEK implants was evaluated together with in vivo mechanical stimulation to simultaneously achieve good implantation safety and osseointegration, as validated by good clinical outcomes.

Despite the potential for improved osseointegration, the wider application of porous PEEK implants has been hindered by the major concern of a decrease in its mechanical properties through the construction of porous structures. The elastic modulus and the yield strength of the solid PEEK structure ($E$=1305 MPa; $\sigma_s$=148 MPa) were superior to those of cancellous bone ($E$=20–500 MPa; $\sigma_s$=4–12 MPa) and

lower than those of cortical bone ($E$=3000–30 000 MPa; $\sigma_s$= 130–180 MPa) [13]. For the solid PEEK prostheses used in bone reconstruction in the high load-bearing area, such as hip implants, rib prostheses, and mandibular implants, the safety factor was 2–3 according to previous research [23, 33, 34]. Considering the lower mechanical properties of the porous PEEK structure ($E$=127–551 MPa; $\sigma_s$=10–41 MPa), the application of porous PEEK prostheses in the high load-bearing area requires further careful considerations on safety and stability. Generally, porous PEEK prostheses are more suitable for reconstruction in the low load-bearing area, such as the maxillofacial bone. Therefore, a paranasal defect was selected with screw preloads used as major loads. Porous PEEK prostheses became more sensitive to the loads with increasing pore size, with a noticeable decrease in the safety factor due to a slight increase in preload, emphasizing the importance of considering the characteristics of the loading environment during the porous structure design.

In addition to mechanical safety, bone growth and osseointegration are other key factors for the design of the porous structure of PEEK implants. In this study, the influence of the pore size on bone growth was investigated based on Wolff's law, and the osteointegration of porous PEEK implants was improved by environmental mechanical regulation. According to previous research, pore size affects bone growth by affecting osteocyte behavior and nutrient transport [35]. The pore size of 600 μm was found to achieve high fixation ability and deep bone in-growth in the early period [36], as well as to improve osteoinduction [37] and neovascularization [38]. Therefore, a pore size of 600 μm was selected in this study, while an alternative pore size could also achieve a high percentage of effective bone growth area of the bone-implant interface with appropriate preloads. Apart from pore size, other design parameters of the porous structure, such as the pore architecture [39] or pore distribution [40], affect bone growth and could be regulated for better implant performance.

The mechanical environment of the implant-bone interface was adjusted in a controlled manner by combined control of pore structure and preload to optimize bone growth rate at the interface. Active regulation of in vivo mechanical stimulation has important clinical significance for cases where the normal physiological load is not enough for mechanical stimulation for bone growth after implantation, similar to the effect of the stress shielding associated with metal implants. Here, we achieved active regulation of in vivo mechanical stimulation through the application of screw preloads to improve interfacial bone growth. The stability of the screw connection needs to be concerned in the regulation of the screw preloads. As shown in Sect. 3.3, the trends for change in the effective bone growth area at the bone-implant interface and the bone-screw interface were inconsistent and a trade-off is necessary.

Our optimized design resulted in good clinical outcomes and osseointegration performance of the 3D-printed porous PEEK implants; further, we observed high consistency for promoted/inhibited bone growth areas between the FE analysis and clinical data. Based on CT images, bone growth at the bone-implant interface of the patients using 3D-printed solid PEEK implants was not appropriate despite greater preloads. This does not benefit long-term bone regeneration and may further lead to osteoporosis. The unsatisfactory bone repair efficacy of 3D-printed solid PEEK implants may be due to the bioinert nature of PEEK, which makes it difficult for bone cells to attach and hinders bone tissue growth. Compared to solid PEEK implants, the interconnected porous structure of porous PEEK implants mimicked the extracellular matrix of the native bone tissues and provided space for bone in-growth, with BV/TV reaching 42.2% at 3 months after implantation and 59.9% at 6 months after implantation. The integration between the porous structure and new bone improved the interfacial mechanical locking, which contributed to the long-term stability of the implants. Furthermore, the mechanical properties of PEEK implants could be further improved with new bone formation, according to a previous study [41]. In summary, the present clinical results validated the benefit of a porous structure for bone growth and osseointegration, highlighting the obvious potential of 3D-printed porous PEEK implants in maxillofacial repair and reconstruction.

In the FE model in this study, we made some simplifications of the geometry and boundary conditions. For example, we used equivalent material properties of porous PEEK structures. In the future, a more detailed FE model could be built to investigate the mechanical behavior of the individual cell unit of the porous structure. Different pore architectures and pore distributions, such as the Voronoi-based architecture and the anisotropic pore distribution [42], which have attracted much attention in recent years, can be considered for a future porous PEEK implant design. Furthermore, the combination of a porous structure design and material modification will be an important development direction for PEEK implants. A PEEK composite with reinforcing fibers can also help overcome the problems associated with weak mechanical properties of the porous PEEK structures [43].

## 5 Conclusions

Despite their potential advantages in osteointegration, porous PEEK implants are clinically limited due to safety concerns regarding mechanical stability. In this study, implantation safety and good osteointegration of porous PEEK implants were achieved by combined regulation of pore structure and in vivo mechanical stimulation. Clinical applications of 3D-printed porous PEEK implants demonstrated optimal

bone repair efficacy and excellent osseointegration, indicating long-term stability, compared to solid PEEK implants, validating the clinical feasibility of porous PEEK implants. The design strategy for porous PEEK implants used here paves the way for the development and clinical application of other types of prostheses in PEEK.

**Acknowledgements** The work was supported by the National Key R&D Program of China (No. 2023YFB4603500), the Program for Innovation Team of Shaanxi Province (No. 2023-CX-TD-17), the Fundamental Research Funds for the Central Universities, and the Shaanxi Province Qinchuangyuan "Scientist + Engineer" Team Construction Project (No. 2022KXJ-106).

**Author contributions** YJL: original draft, design and manufacturing. LW: original draft, conceptualization. DCL: conceptualization. JZ and SGL: clinical applications. JBZ, JFK, ECD, CNS, RHA, CZL, and CCY: methods.

## Declarations

**Conflict of interest** CZL is an editorial board member for *Bio-Design and Manufacturing* and was not involved in the editorial review or the decision to publish this article. The authors declare that they have no conflict of interest.

**Ethical approval** This research has been approved by the Stomatological Hospital, Southern Medical University. The 3D-printed PEEK implants were approved by the State Key Laboratory for Manufacturing Systems Engineering, Xi'an Jiaotong University. The study was performed by the Declaration of Helsinki's ethical principles and international norms and was approved by the Ethics Committee of the Hospital (EC-CT-[2019]28). All subjects signed a written informed consent before their inclusion in the study.

## References

1. Hacherl CC, Patel NA, Jones K et al (2021) Characterizing adverse events of cranioplasty implants after craniectomy: a retrospective review of the federal manufacturer and user facility device experience database. Cureus 13(7):e16795. https://doi.org/10.7759/cureus.16795
2. Wang L, Yang CC, Sun CN et al (2022) Fused deposition modeling PEEK implants for personalized surgical application: from clinical need to biofabrication. Int J Bioprint 8(4):615. https://doi.org/10.18063/ijb.v8i4.615
3. Kauke-Navarro M, Knoedler L, Knoedler S et al (2024) Surface modification of PEEK implants for craniofacial reconstruction and aesthetic augmentation-fiction or reality? Front Surg 11:1351749. https://doi.org/10.3389/fsurg.2024.1351749
4. Sakkas A, Wilde F, Heufelder M et al (2017) Autogenous bone grafts in oral implantology—is it still a "gold standard"? A consecutive review of 279 patients with 456 clinical procedures. Int J Implant Dent 3(1):23. https://doi.org/10.1186/s40729-017-0084-4
5. Panayotov IV, Orti V, Cuisinier F et al (2016) Polyetheretherketone (PEEK) for medical applications. J Mater Sci Mater Med 27(7):118. https://doi.org/10.1007/s10856-016-5731-4
6. Zheng Z, Liu PJ, Zhang XM et al (2022) Strategies to improve bioactive and antibacterial properties of polyetheretherketone (PEEK) for use as orthopedic implants. Mater Today Bio 16: 100402. https://doi.org/10.1016/j.mtbio.2022.100402
7. Bartelstein MK, Van Citters DW, Weiser MC et al (2017) Failure of a polyaryletheretherketone-cobalt-chromium composite femoral stem due to coating separation and subsidence: a case report. JBJS Case Connect 7(4):e83. https://doi.org/10.2106/jbjs.Cc.16.00280
8. Evans NT, Torstrick FB, Lee CSD et al (2015) High-strength, surface-porous polyether-ether-ketone for load-bearing orthopedic implants. Acta Biomater 13:159–167. https://doi.org/10.1016/j.actbio.2014.11.030
9. Yang Q, Zhang GC, Ma ZL et al (2015) Effects of processing parameters and thermal history on microcellular foaming behaviors of PEEK using supercritical $CO_2$. J Appl Polym Sci 132(39): 42576. https://doi.org/10.1002/app.42576
10. Zhao Y, Wong HM, Wang WH et al (2013) Cytocompatibility, osseointegration, and bioactivity of three-dimensional porous and nanostructured network on polyetheretherketone. Biomaterials 34(37):9264–9277. https://doi.org/10.1016/j.biomaterials.2013.08.071
11. Zheng JB, Zhao HY, Dong EC et al (2021) Additively-manufactured PEEK/HA porous scaffolds with highly-controllable mechanical properties and excellent biocompatibility. Mater Sci Eng C Mater Biol Appl 128:112333. https://doi.org/10.1016/j.msec.2021.112333
12. Wang HZ, Chen P, Wu HZ et al (2022) Comparative evaluation of printability and compression properties of poly-ether-ether-ketone triply periodic minimal surface scaffolds fabricated by laser powder bed fusion. Addit Manuf 57:102961. https://doi.org/10.1016/j.addma.2022.102961
13. Azami M, Moztarzadeh F, Tahriri M (2010) Preparation, characterization and mechanical properties of controlled porous gelatin/hydroxyapatite nanocomposite through layer solvent casting combined with freeze-drying and lamination techniques. J Porous Mater 17(3):313–320. https://doi.org/10.1007/s10934-009-9294-3
14. Gummadi SK, Saini A, Owusu-Danquah JS et al (2022) Mechanical properties of 3D-printed porous poly-ether-ether-ketone (PEEK) orthopedic scaffolds. JOM 74(9):3379–3391. https://doi.org/10.1007/s11837-022-05361-6
15. Du XY, Ronayne S, Lee SS et al (2023) 3D-printed PEEK/silicon nitride scaffolds with a triply periodic minimal surface structure for spinal fusion implants. ACS Appl Bio Mater 6(8):3319–3329. https://doi.org/10.1021/acsabm.3c00383
16. Spece H, Yu T, Law AW et al (2020) 3D printed porous PEEK created via fused filament fabrication for osteoconductive orthopaedic surfaces. J Mech Behav Biomed Mater 109:103850. https://doi.org/10.1016/j.jmbbm.2020.103850
17. Jia CQ, Zhang Z, Cao SQ et al (2023) A biomimetic gradient porous cage with a micro-structure for enhancing mechanical properties and accelerating osseointegration in spinal fusion. Bioact Mater 23:234–246. https://doi.org/10.1016/j.bioactmat.2022.11.003
18. Roskies M, Jordan JO, Fang DD et al (2016) Improving PEEK bioactivity for craniofacial reconstruction using a 3D printed scaffold embedded with mesenchymal stem cells. J Biomater Appl 31(1):132–139. https://doi.org/10.1177/0885328216638636
19. Cowin SC, Moss-Salentijn L, Moss ML (1991) Candidates for the mechanosensory system in bone. J Biomech Eng 113(2):191–197. https://doi.org/10.1115/1.2891234
20. Patel K, Brandstetter K (2016) Solid implants in facial plastic

surgery: potential complications and how to prevent them. Facial Plast Surg 32(5):520–531. https://doi.org/10.1055/s-0036-1586497
21. Lee TY, Chung HY, Dhong ES et al (2019) Paranasal augmentation using multi-folded expanded polytetrafluorethylene (ePTFE) in the East Asian nose. Aesthet Surg J 39(12):1319–1328. https://doi.org/10.1093/asj/sjz103
22. Nocini PF, Boccieri A, Bertossi D (2009) Gridplan midfacial analysis for alloplastic implants at the time of jaw surgery. Plast Reconstr Surg 123(2):670–679. https://doi.org/10.1097/PRS.0b013e318196b958
23. Kang JF, Zhang J, Zheng JB et al (2021) 3D-printed PEEK implant for mandibular defects repair-a new method. J Mech Behav Biomed Mater 116:104335. https://doi.org/10.1016/j.jmbbm.2021.104335
24. Wang L, Kang JF, Sun CN et al (2017) Mapping porous microstructures to yield desired mechanical properties for application in 3D printed bone scaffolds and orthopaedic implants. Mater Des 133:62–68. https://doi.org/10.1016/j.matdes.2017.07.021
25. Sun CN, Wang L, Kang JF et al (2018) Biomechanical optimization of elastic modulus distribution in porous femoral stem for artificial hip joints. J Bionic Eng 15(4):693–702. https://doi.org/10.1007/s42235-018-0057-1
26. Wang D, Qu A, Zhou H et al (2016) Biomechanical analysis of the application of zygoma implants for prosthesis in unilateral maxillary defect. J Mech Med Biol 16(8):1640030. https://doi.org/10.1142/s0219519416400303
27. Miyamoto S, Ujigawa K, Kizu Y et al (2010) Biomechanical three-dimensional finite-element analysis of maxillary prostheses with implants. Design of number and position of implants for maxillary prostheses after hemimaxillectomy. Int J Oral Maxillofac Surg 39(11):1120–1126. https://doi.org/10.1016/j.ijom.2010.06.011
28. Zhang J, Li DC, Liu YJ et al (2022) Application of patient-specific PEEK implant for aesthetic considerations in paranasal augmentation. J Craniofac Surg 33(8):e877–e880. https://doi.org/10.1097/scs.0000000000008824
29. Monje A, Ravidà A, Wang HL et al (2019) Relationship between primary/mechanical and secondary/biological implant stability. Int J Oral Maxillofac Implants 34:s7–s23. https://doi.org/10.11607/jomi.19suppl.g1
30. Sharma N, Welker D, Aghlmandi S et al (2021) A multi-criteria assessment strategy for 3D printed porous polyetheretherketone (PEEK) patient-specific implants for orbital wall reconstruction. J Clin Med 10(16):3563. https://doi.org/10.3390/jcm10163563
31. Torstrick FB, Safranski DL, Burkus JK et al (2017) Getting PEEK to stick to bone: the development of porous PEEK for interbody fusion devices. Tech Orthop 32(3):158–166. https://doi.org/10.1097/bto.0000000000000242
32. Moiduddin K, Mian SH, Elseufy SM et al (2023) Polyether-ether-ketone (PEEK) and its 3D-printed quantitate assessment in cranial reconstruction. J Funct Biomater 14(8):429. https://doi.org/10.3390/jfb14080429
33. Belwanshi M, Jayaswal P, Aherwar A (2022) Mechanical behaviour investigation of PEEK coated titanium alloys for hip arthroplasty using finite element analysis. Mater Today Proc 56(5): 2808–2817. https://doi.org/10.1016/j.matpr.2021.10.112
34. Kang JF, Wang L, Yang CC et al (2018) Custom design and biomechanical analysis of 3D-printed PEEK rib prostheses. Biomech Model Mechanobiol 17(4):1083–1092. https://doi.org/10.1007/s10237-018-1015-x
35. Bružauskaitė I, Bironaitė D, Bagdonas E et al (2016) Scaffolds and cells for tissue regeneration: different scaffold pore sizes—different cell effects. Cytotechnology 68(3):355–369. https://doi.org/10.1007/s10616-015-9895-4
36. Taniguchi N, Fujibayashi S, Takemoto M et al (2016) Effect of pore size on bone ingrowth into porous titanium implants fabricated by additive manufacturing: an in vivo experiment. Mater Sci Eng C Mater Biol Appl 59:690–701. https://doi.org/10.1016/j.msec.2015.10.069
37. Fukuda A, Takemoto M, Saito T et al (2011) Osteoinduction of porous Ti implants with a channel structure fabricated by selective laser melting. Acta Biomater 7(5):2327–2336. https://doi.org/10.1016/j.actbio.2011.01.037
38. Bai F, Zhang JK, Wang Z et al (2011) The effect of pore size on tissue ingrowth and neovascularization in porous bioceramics of controlled architecture in vivo. Biomed Mater 6(1):015007. https://doi.org/10.1088/1748-6041/6/1/015007
39. Zadpoor AA (2015) Bone tissue regeneration: the role of scaffold geometry. Biomater Sci 3(2):231–245. https://doi.org/10.1039/c4bm00291a
40. Nune KC, Kumar A, Misra RDK et al (2017) Functional response of osteoblasts in functionally gradient titanium alloy mesh arrays processed by 3D additive manufacturing. Colloids Surf B Biointerfaces 150:78–88. https://doi.org/10.1016/j.colsurfb.2016.09.050
41. Zheng JB, Zhao HY, Ouyang ZC et al (2022) Additively-manufactured PEEK/HA porous scaffolds with excellent osteogenesis for bone tissue repairing. Compos Part B Eng 232:109508. https://doi.org/10.1016/j.compositesb.2021.109508
42. Gómez S, Vlad MD, López J et al (2016) Design and properties of 3D scaffolds for bone tissue engineering. Acta Biomater 42: 341–350. https://doi.org/10.1016/j.actbio.2016.06.032
43. Lu SW, Zhang BN, Niu JY et al (2024) Effect of fiber content on mechanical properties of carbon fiber-reinforced polyether-ether-ketone composites prepared using screw extrusion-based online mixing 3D printing. Addit Manuf 80:103976. https://doi.org/10.1016/j.addma.2024.103976